Comparisons of TEC Gradients Derived from Several GNSS-Based Approaches

Xiaoqing Pi
Jet Propulsion Laboratory, California Institute of Technology, Pasadena, CA, USA

BIOGRAPHIES

Dr. Xiaoqing Pi joined NASA's Jet Propulsion Laboratory, California Institute of Technology, in 1996. His primary research interests include ionospheric remote sensing and modeling, coupling of magnetosphere-ionosphere-thermosphere, and space weather effects on the ionosphere. He has conducted a variety of developments for modeling and measuring the ionosphere, including Global Assimilative Ionospheric Model (GAIM), Global Map of Ionospheric Irregularities (GMIIS), ionospheric Multimodel Ensemble Prediction System (iMEPS), the rate of TEC index (ROTI), small-scale TEC slopes (SSTS) and small-scale TEC irregularities (SSTI), medium-scale TEC gradients (MSTG), combined global TEC gradients (CGTG), plasmaspheric measurements from low Earth orbiters, and machine-learning prediction of regional ionospheric irregularities and scintillation (ML-PRIIS).

ABSTRACT

In this paper several methods are described for measuring spatial slopes of ionospheric total electron content (TEC) using ground-based GNSS observations. The following approaches are included: (1) Global Ionospheric Map (GIM) based TEC gradients (GBTG); (2) small-scale TEC slopes (SSTS); (3) averaged TEC and gradients (ATAG); (4) fitted IGP TEC and gradients (FITG). Characteristics of TEC slopes resulted from these approaches with regionally distributed GNSS data in different latitude regions are assessed and compared. In addition, a new way to measure small-scale TEC irregularities (SSTI) is defined as the standard deviation of detrended SSTS, which characterizes ionospheric irregularities at horizontal spatial scales ranging from 1.8 to 15 km approximately. Examples of global images of TEC slopes and SSTI are presented, which are obtained using data from thousands of globally distributed GNSS stations. A preliminary analysis indicates that the magnitude and direction of TEC slopes derived using these approaches are consistent in general, but differences among the approaches become noticeable when the ionosphere is perturbed either during active space weather or irregularity events. The differences between SSTS, ATAG and FITG are attributed to the data distribution and amount in the binned area that may affect 2-dimensional data fitting, errors of satellite and receiver instrumental bias estimation, and data outliers which must be detected and removed.

1. INTRODUCTION

Undetected large TEC spatial variations in short distance is a threat to navigation systems including satellite-based augmentation system (SBAS) or ground-based augmentation system (GBAS). The augmentation systems provide wide- or local-area ionospheric corrections to users for precise positioning, and the systems are required to bound possible errors due to such TEC spatial variations. In Earth remote sensing observations, image processing using data collected from space-borne interferometric synthetic aperture radar (InSAR) needs to deal with ionospheric TEC changes including small-scale irregularities in directions along (azimuth) and cross (range) satellite orbit track. TEC variations in these directions can cause signal phase and range changes that, if not removed, distort remote sensing images.

GNSS is a unique system useful to measuring such TEC variations. TEC slope, defined as the vertical TEC change divided by distance between the locations of two ionospheric piercing points (IPPs) at a fixed height, can be obtained using a dual-frequency ground-based receiver that tracks multiple GNSS satellites. TEC data sampled at 1-second to 30-second intervals allows measurements of TEC slopes in relatively short distances along IPP tracks of GNSS satellite orbit (along-track hereafter). On the other hand, TEC slopes can also be measured from cross-satellite (different satellites tracked by the same single receiver) or cross-receiver (different receivers tracking the same satellite) (briefly cross-track hereafter) data samples.

 https://doi.org/10.33012/2022.18198

This paper first describes several methods to deriving TEC slopes in latitude and longitude directions using GNSS data. The methods include: (1) Global Ionospheric Map (GIM) based TEC gradients (GBTG); (2) small-scale TEC slopes (SSTS); (3) averaged TEC and gradients (ATAG); (4) fitted IGP TEC and gradients (FITG). Comparisons are then made to assess characteristics and differences of TEC slopes derived using these approaches. The GBTG and SSTS methods have been described in a previous ION-ITM paper [1] (in which small-scale TEC spatial rate, STSR, was used as a name to represent the measurements of local TEC slopes but it is now renamed SSTS), and they are summarized here for comparisons with the other methods. In addition, the standard deviation of detrended SSTS is defined as a new way to measure small-scale TEC irregularities (SSTI) at horizontal spatial scales ranging from 1.8 to 15 km approximately.

One should keep in mind that some factors besides data noise have impact on TEC slope measurements, including errors of receiver and transmitter instrumental bias estimation as well as TEC slant-to-vertical conversion error. This particularly concerns cross-track differential TEC slope measurements since the bias estimation errors and observation elevations can be different between cross-track receivers and/or satellites, and data noise levels can also be different between receivers.

The four methods of estimating TEC slopes and the approach to measuring SSTI are described in the next section. Examples of TEC slopes and SSTI are shown visually to examine regional features in a global context. Differences between TEC slopes obtain using these methods with regionally and globally distributed GNSS data are also examined. The impact of space weather and ionospheric irregularities on TEC slopes is also presented by comparing quiet-time and storm-time TEC slopes.

2. METHODS OF DERIVING TEC SLOPES FROM GNSS DATA

The four approaches to deriving TEC slopes are based on different techniques that map, fit or average GNSS-TEC observations on global or local grid. They all involve vertical-to-slant conversion using a widely-used mapping function for spherical geometry, i.e.,

$$\mathrm{M} = \sqrt{1 - \left(\frac{\cos e}{1 + \frac{h_i}{r_e}} \right)^2}^{-1} \tag{1}$$

where M is the factor for vertical-to-slant conversion, e is the receiver-to-satellite observation elevation angle, h_i is the ionospheric shell height, and r_e is the Earth radius. For slant-to-vertical TEC mapping, h_i is chosen to be 450 km, and the mapped vertical TEC is set to the projected IPP geolocation of the radio signal. Note that this mapping function assumes a spherical shell ionosphere or horizontally uniform TEC in the region. This assumption breaks down in regions where large TEC gradient exists, and the conversion introduces an error that is larger at lower elevation angle. A general form of conversion between slant observation and vertical TEC for a single receiver-satellite pair can be expressed as follows:

$$\mathrm{sTEC}_{obs} = \mathrm{M\ TEC} + b_r + b_t, \tag{2}$$

where sTEC_{obs} is the slant observation, TEC stands for vertical TEC, b_r and b_t denote the receiver and transmitter interfrequency biases, respectively. Errors due to data noise and other factors are neglected in equation (2) for simplicity.

Note that M needs to be applied with or after removal of the instrument biases in general. However, the biases can be eliminated if differential TEC is measured in a short distance along the same receiver-to-satellite track. To obtain differential TEC in different methods that use either along-track or/and cross-track data, the GPS transmitter biases are removed using the JPL GIM solutions [2][3][4]. The receiver bias for any receiver can be solved through the following equation, i.e.,

$$b_r^i = \mathrm{sTEC}_{obs}^{i,j} - b_t^j - \mathrm{M\ TEC}, \tag{3}$$

where superscripts i and j stand for ith receiver and jth satellite, TEC is computed using GIM. Further descriptions of this approach are referred to [1].

2.1 GIM-Based TEC Gradients (GBTG)

As described in [1], GIM can be used to estimate TEC gradient components on large scales (greater than 300 km) in latitude and longitude directions. Briefly, TEC gradient can be expressed in spherical coordinate system as follows,

$$\nabla \mathrm{TEC}(\theta', \phi) = \frac{\partial \mathrm{TEC}}{r\partial\theta'}\mathbf{e}_\theta + \frac{\partial \mathrm{TEC}}{r\sin(\theta')\partial\phi}\mathbf{e}_\phi. \tag{4}$$

where θ' and ϕ denote co-latitude and longitude (θ denotes latitude). The two terms on the righthand side of the equation give TEC gradient components in co-latitude and longitude direction, respectively. In this analysis the positive latitude gradient is defined in the northward direction, which is in the opposite direction of co-latitude gradient. With GIM TEC data, the TEC gradient components can be computed as $\mathrm{dTEC}_\theta/\mathrm{dS}_\theta$ and $\mathrm{dTEC}_\phi/\mathrm{dS}_\phi$, respectively, dS_θ and dS_ϕ denote the arc lengths in latitude and longitude directions between two IPPs. An example of TEC gradient components computed using GIM TEC was given in [1]. Here GBTG for a 15-min interval during 17 March 2015 is given in Figures 1a and 1b. The two components are computed using GIM with spatial resolutions of 1°×1° (longitude × latitude) and radius at r_e + 450 km (ionospheric shell altitude). It is apparent that the magnitude of latitude gradient is much larger than that of longitude gradient, and the former is more structured at low latitudes than the latter. This is due to the equatorial ionospheric anomaly (EIA) phenomenon, which often presents TEC peaks at geomagnetic latitudes about 15° to 18° off the geomagnetic equator in both hemispheres.

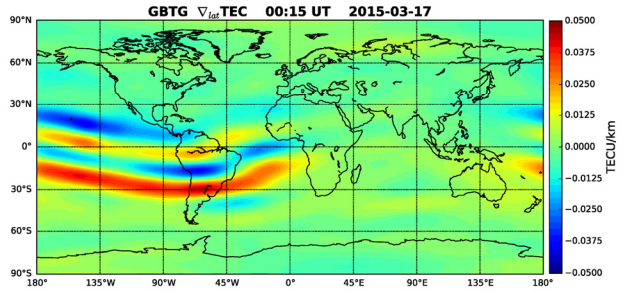

Figure 1a. Global ∇_θTEC computed from GIM for 00:15 UTC during 17 March 2015.

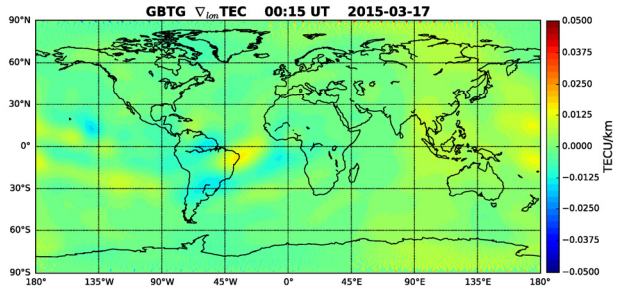

Figure 1b. Global ∇_ϕTEC computed from GIM for 00:15 UTC during 17 March 2015.

TEC slopes in an arbitrary direction can be estimated by projecting the two gradients to the specific direction. In general, GBTG is based on large-scale TEC mapping. It likely smooths out the medium- and small-scale structures. Different approaches are necessary in order to address TEC slopes at scales from a few hundred kilometers to a few kilometers.

2.2 Small-Scale TEC Slopes (SSTS) and Small-Scale TEC Irregularities (SSTI)

The method of SSTS is used to measure TEC slopes at scales ranging from 1.8 to 15 km (IPP spacing) approximately. The detailed method has been described in [1], in which a name "small-scale TEC spatial rate (STSR)" is used that is renamed SSTS here. Briefly SSTS is computed from TEC data along IPP tracks of GNSS observations, i.e.,

$$\mathrm{SSTS} = d\mathrm{TEC}/dS, \tag{5}$$
$$\mathrm{SSTS}_{\theta'} = (d\mathrm{TEC}/dS)\sin(\gamma), \tag{6}$$
$$\mathrm{SSTS}_{\phi} = (\mathrm{dTEC}/dS)\cos(\gamma), \tag{7}$$
$$\gamma = \arctan\left(\frac{rd\theta'}{rsin(\theta')d\phi}\right) \tag{8}$$

where dTEC and dS are the differential TEC and the distance between two IPPs, respectively, along the same satellite track. Several advantages of measuring SSTS are listed here: (1) measuring dTEC exclusively along the same receiver-satellite track helps to eliminate the bias estimation errors; (2) projection of SSTS to latitude and longitude directions helps to characterize TEC changes in the two directions in which the ionosphere varies quite differently at least at middle and low latitude; (3) the latitude and longitude components can be used to estimate dTEC/dS in other directions. Note that dTEC is obtained based on

slant-to-vertical mapping, which is an approximation and may be affected by the mapping function error at low elevation angles. Keep in mind that measurements taken consecutively for a certain time interval involve also TEC temporal variations, but such temporal variations are small if data is sampled at 30 seconds or shorter intervals.

When ionospheric irregularities are present, small-scale TEC irregularities (SSTI) can be measured by removing the variation trend of SSTS and computing the standard deviation of the residuals. In examples to be presented next, the detrending is performed by a linear least-squares fit of the 30-sec sampled along-track SSTS data in a 5-min interval over the distances of the dTEC IPP centers from the starting point of the interval. SSTI is then defined as the standard deviation of all detrended SSTS data along multiple satellite tracks during the 5-min interval within a latitude-longitude bin, i.e.,

$$\mathrm{SSTI} = \sqrt{\frac{1}{N-1}\sum_{i=1}^{N}(\mathrm{SSTS}'_i - \langle \mathrm{SSTS}' \rangle)^2}, \tag{9}$$

where SSTS′ is the detrended SSTS in the bin, and <SSTS′> is the assemble average of all SSTS′ data in the bin. Figure 2 shows an example of SSTS and SSTS′ measured from station 0000 tracking GPS satellite 23 during 17 March 2015. In this data set, TEC at low latitudes shows large slopes vs. latitude (lower left panel). IPP arc length (or distance, lower middle panel) of differential TEC (upper middle panel) varies between 4 km and 10.5 km. Along-track dTEC/dS shows large variations (red in upper right panel). The detrended dTEC/dS data (upper right, blue) is projected to latitude and longitude directions (lower right panel), respectively, showing larger slopes in latitude direction than in longitude direction.

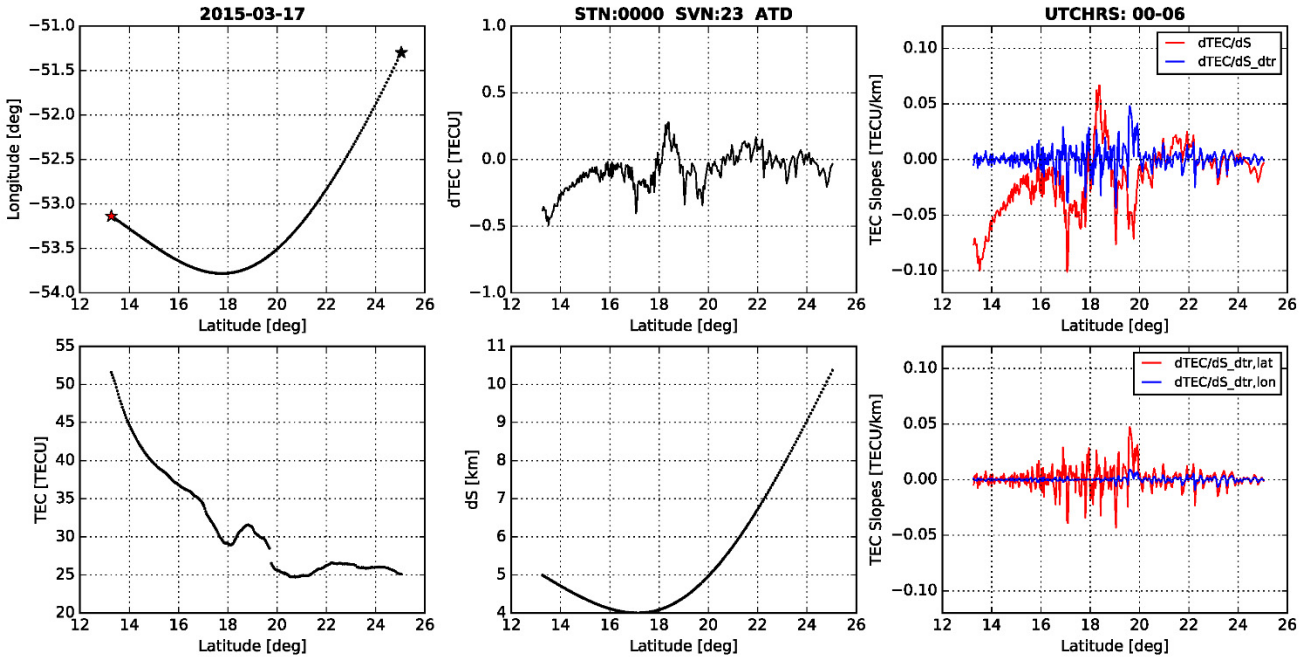

Figure 2. An example of SSTS (red) and detrended SSTS (blue) is shown in the upper right panel. The GNSS data is collected from station 0000 tracking GPS satellite 23, made during 17 March 2017. Upper left: GPS tracking trajectory; lower left: vertical TEC; upper middle: differential TEC measured along the IPP track; lower left: IPP arc lengths (or distances) of the adjacent measurements; lower right: detrended dTEC/dS projected to latitude (red) and longitude (blue) direction, respectively. The red star in the trajectory panel marks the starting point of the observation, while the black star marks the ending point.

Figures 3 and 4 show examples of global SSTS and SSTI maps for latitude and longitude component, respectively, for 00:05:00 UT on 17 March 2015. The SSTS maps are constructed with GPS data from globally-distributed 5,383 stations at 2.5°×3.75° (latitude × longitude) bins. One can identify ionospheric irregularities in SSTI maps in places where SSTI values are apparently

higher than zero. At low latitudes increased SSTI is present in the longitude regions of evening and night sectors, where scintillation often occurs in this season.

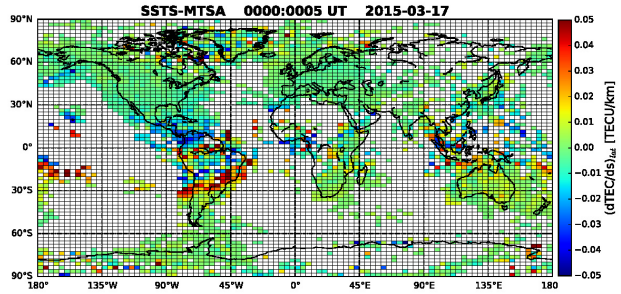

Figure 3a. A global SSTS map (latitude component) for 00:05 UTC 17 March 2015.

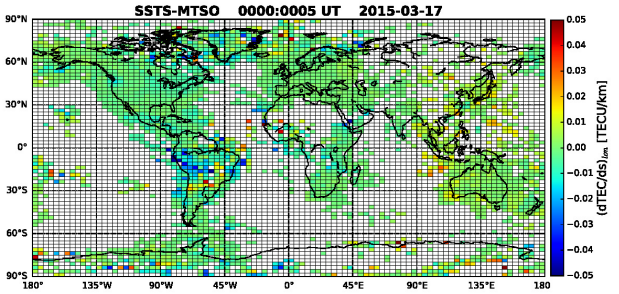

Figure 3b. A global SSTS map (longitude component) for 00:05 UTC 17 March 2015.

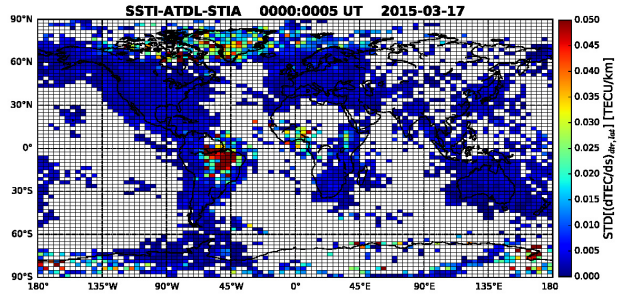

Figure 4a. A global SSTI map (latitude component) for 00:05 UTC 17 March 2015.

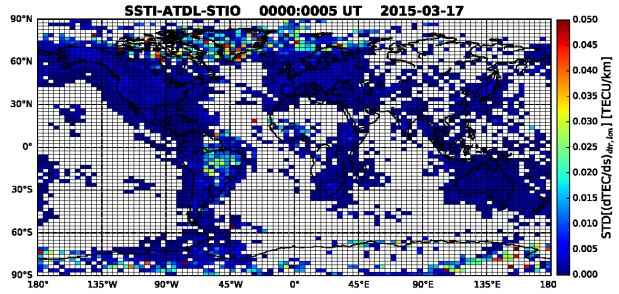

Figure 4b. A global SSTI map (longitude component) for 00:05 UTC 17 March 2015.

2.3 Averaged TEC and Gradients (ATAG)

With TEC obtained from distributed stations, an averaged TEC value can be computed with data within a local latitude and longitude bin. For the bin size used in SSTS, ATAG measured medium-scale TEC gradients (MSTG). With the averaged TEC in adjacent bins in each of latitude and longitude direction, TEC gradient components can be computed. Figures 5a and 5b show global TEC and TEC latitude gradient maps derived from the same GPS data used in producing SSTS and SSTI shown in Figures 3 and 4. Note that the number of bins with data for TEC gradient in latitude direction (TGLA) is smaller than that for TEC since it takes two adjacent TEC values to obtain one TEC gradient.

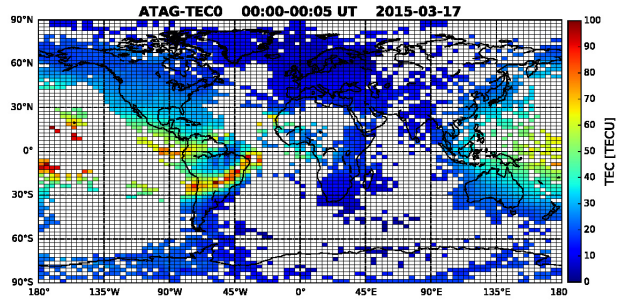

Figure 5a. A global TEC map derived using the ATAG method for 00:05 UTC 17 March 2015.

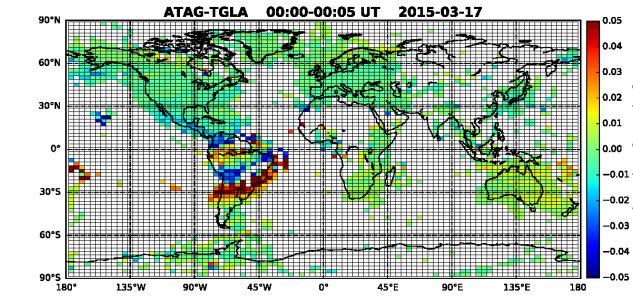

Figure 5b. A global TEC gradient map (latitude direction) derived using the ATAG method for 00:05 UTC 17 March 2015.

2.4 Fitted IGP TEC Gradients (FITG)

FITG is the fourth method presented here. This approach is applied to estimating vertical TEC and TEC gradient components (latitude and longitude) at any ionospheric grid point (IGP) with surrounding slant TEC measurements. FITG applies the Taylor expansion to TEC in equation (2), i.e.,

$$\mathrm{sTEC}(x,y)_{\mathrm{obs}} = \mathrm{M}\left[\mathrm{TEC}(x_0,y_0) + \frac{\partial \mathrm{TEC}}{\partial x}dx + \frac{\partial \mathrm{TEC}}{\partial y}dy\right], \tag{9}$$

where $\mathrm{sTEC}_{\mathrm{obs}}$ is the bias-removed slant TEC observation, x and y are the local Cartesian coordinates of the IPP on the ionospheric shell treated approximately as a plain centered at x_0 and y_0, and $dx = x - x_0$ and $dy = y - y_0$ are the distance in x (longitude) and y (latitude) direction from the local origin. With a number of sTEC measurements surrounding the IGP in a circle with a radius r_c, TEC(x_0, y_0), ∂TEC/∂x and ∂TEC/∂y can be solved for using least-squares fitting. The number of slant TEC measurements is affected by r_c, which affects the spatial resolution of the solution and the smoothness of the solutions if FITG is applied to a number of IGPs in a region. Figures 6a and 6b give an example of TEC and TEC gradients obtained using FITG with r_c= 300 km. TEC and gradient for r_c= 100 km and 200 km are also estimated using FITG (not shown here), and their solutions cover less areas due to less data samples in bins where data distribution is relatively sparse. With these radii, the FITG approach measures medium-scale TEC gradients (MSTG), In Figures 6a and 6b TEC and gradient (latitude) values are color-coded and displayed in each bin. The least-squares fit has been applied to obtain TEC measurements for WAAS threat model [5]. It has also been applied to obtain TEC gradient [6].

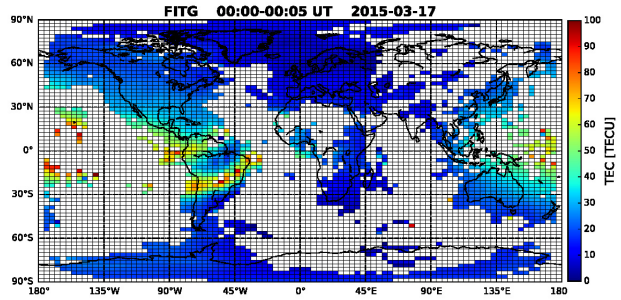

Figure 6a. A global TEC map derived using the FITG method for 00:05 UTC 17 March 2015.

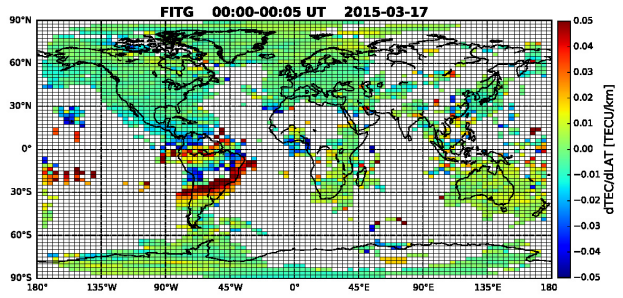

Figure 6b. A global TEC gradient map (latitude direction) derived using the FITG method for 00:05 UTC 17 March 2015.

3. COMPARISONS OF TEC SLOPES ESTIMATED USING DIFFERENT METHODS

As described in 2.1, GBTG may smooth out some ionospheric structures since it is based on large-scale TEC mapping. The ATAG and FITG approaches make use of local data to derive TEC and gradients, and SSTS uses local along-track data exclusively to compute TEC slopes. In this section TEC slopes are compared between the global mapping and local average or fitting to assess the impact of different techniques on TEC slope measurements. To compare the results of four approaches, a same global 2.5°×3.75° (latitude × longitude) grid is used for four approaches. For each data bin, GNSS TEC data, or GIM TEC at 1°×1° (latitude × longitude), is used to compute TEC slopes through average or the least-squares fitting. The temporal resolution of SSTS and MSTG including ATAG and FITG is 5 minutes while it is 15 minutes for GBTG, which is determined by GIM. Two examples of TEC slope comparisons are shown in Figures 7a and 7b showing results at the two locations, one in North America (39°N, 89°W, middle latitude) and the other in South America (4°S, 63°W, low latitude).

At the middle latitude location (North America), the comparisons show that before 6 UTC on the 2015 St. Patrick's Day, TEC slopes measured using the four methods are consistent and small in general though SSTS_{ϕ} is slightly westward compared with the others. There is a major geomagnetic storm started at about 6 UTC. A special issue of the Journal of Geophysical Research was published about studies of this storm, and readers can find related references following [6]. Some discrepancies in the results of four approaches show up after about 9:30 UTC when ionospheric disturbances developed in different regions:

1. SSTS, ATAG and FITG all show moderate TEC increase towards north during 9-12 UTC, which is very weak or not seen in GBTG.

2. SSTS shows more fluctuations in time sequence than the others.

After 20:30 UTC, all TEC slopes show significant southward and westward disturbances, indicating severe effects of the ionospheric storm in the mid-latitude region.

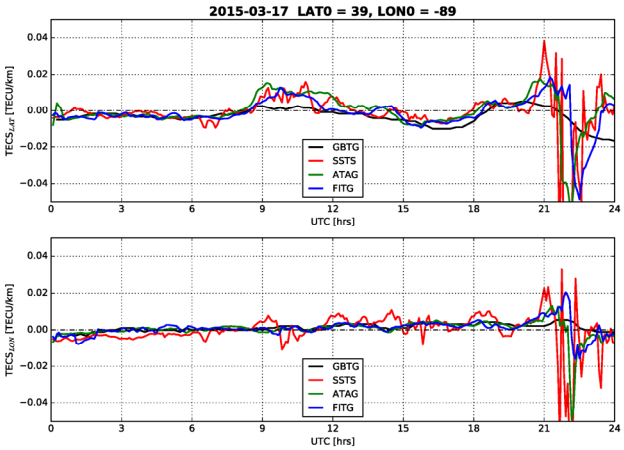

Figure 7a. TEC slopes at 39°N, 89°W (North America) derived using GBTG, SSTS, ATAG and FITG method during 17 March 2015.

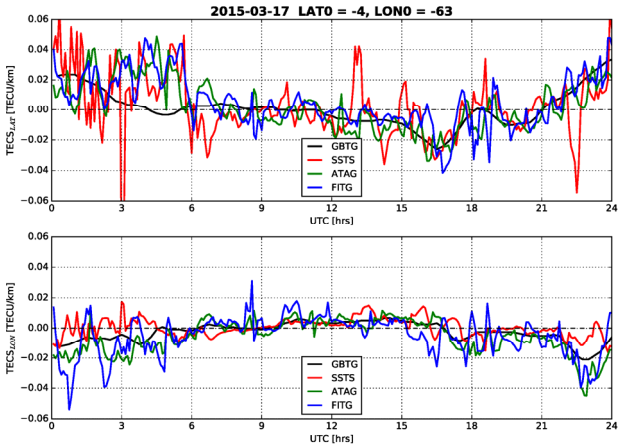

Figure 7b. TEC slopes at 4°S, 63°W (South America) derived using GBTG, SSTS, ATAG and FITG method during 17 March 2015.

At the low latitude (South America, Figure 7b), there are quite some temporal variations in TEC slopes of SSTS, ATAG and FITG particularly before about 7 UTC. These variations appear to be related to ionospheric irregularities as shown in Figures 4a and 4b, which often occur during the evening hours in the South America low-latitude region. The overall trend of temporal variations of the four approaches is similar during most of time. The differences are as follows:

1. The trend of GBTG in latitude direction is different from the others during 4 to 6 UTC.
2. $SSTS_\theta$ shows larger fluctuations in latitude direction than the others.
3. FITG slopes show larger magnitude in longitude direction than ATAG slopes.

The analysis of the four TEC slope results indicates that the slope measurements are affected by the algorithms of different approaches. For example, GIM-based GBTG gives smoothed TEC slopes and it may underestimate the slopes. SSTS is appreciable for its measurements of small spatial scales and particularly for measuring ionospheric irregularities, and for its along-track differential measurements that eliminate bias estimation errors. However, the projection of dTEC/dS to latitude or longitude direction is not exactly same as $dTEC_\theta/dS_\theta$ or $dTEC_\phi/dS_\phi$ as computed in GBTG, ATAG and FITG. SSTS may be more sensitive to outliers, which can cause relatively large errors in the SSTS differential measurements. FITG may be affected by the data distribution in the bin and by data outliers. In ATAG, differential TEC is computed using averaged TEC values in adjacent bins in each of latitude and longitude directions. This method is less susceptible to data noise because of the averaging but its coverage is reduced somewhat since one TEC gradient is obtained from data in two adjacent bins, and its results can still be affected by bias estimation errors for different satellites and receivers. FITG is flexible in setting the radius that encloses data in the area surrounding an IGP. More data samples can be enclosed with a larger radius but a larger radius also means lower spatial resolution in the solution. In addition, FITG solution may also be affected by the bias estimation errors particularly in cross-track data, which may be the reason that its solution shows larger fluctuations than those of ATAG. Further study is needed to reconcile at least the discrepancies of SSTS, ATAG and FITG solutions, and to reduce bias estimation errors and data noise as well as outliers.

4. CONCLUSIONS

Vertical TEC slopes can be approximately measured using bias-removed GNSS TEC data collected from ground-based tracking receivers. TEC data can be averaged for a two-dimensional latitude-longitude bin within a time interval. The averaged TEC data in adjacent bins can then be used to compute TEC gradient between the bins in the corresponding direction. The GBTG and ATAG methods presented in this work are suitable for such TEC gradient measurements. The TEC gradient components can also be obtained using least-squares fitting with slant or vertical TEC data surrounding an IGP. Its solution can be affected by the circular radius that is chosen to enclose the data. The horizontal spatial resolution of the TEC slope measurements

depends on the size of the data bin, which can be 0.5°×0.5° (latitude × longitude) for regions of densely distributed receivers as shown previously in [1] or 2.5°×3.75° globally as demonstrated in this work. Differential TEC can also be obtained along IPP tracks of receiver-to-satellite observations using data between adjacent samples as described in the SSTS approach. The along-track differential TEC measurements eliminate bias estimation errors and provide TEC slopes at about 1.8 km to 15 km scales. This makes detrended SSTS suitable for measuring small-scale TEC irregularities (SSTI) as also demonstrated in this work. SSTS and SSTI can be projected to latitude and longitude directions to characterize slope trends and variations in the two directions. With 30-second sampled data, the temporal resolution of ATAG, FITG, SSTS and SSTI can be 5 minutes, and the resolution of GBTG is 15 minutes determined by the temporal resolution of GIM.

GBTG is based on large-scale TEC mapping and provides global coverage without gaps. Its spatial variation is smooth in general and may underestimate the gradients particularly in regions where large TEC gradient is present, such as in the equatorial ionospheric anomaly (EIA) region. Both ATAG and FITG measure medium-scale TEC gradients (MSTG). ATAG is based on averaged TEC within binned areas. The average helps to reduce the impact of data noise but it is still affected by the errors of satellite and receiver bias estimation, and its spatial coverage is reduced compared to FITG and SSTS since the differential TEC of ATAG computation requires TEC values in two adjacent bins. FITG can be applied to estimation of TEC gradients at IGPs. Its solution is affected by the radius of the circle surrounding the IGP and the bias estimation errors. A larger radius encloses more data and appears to yield more reliable estimation, but the larger radius reduces the spatial resolution and smooths out the structures. SSTS is appreciable for measuring small-scale TEC variations. In SSTS measurements the bias estimation errors are eliminated by the along-track adjacent sampling, but data outliers in differential TEC must be detected and removed to control the data quality. The short IPP spacing (1.8 km to 15 km) makes the detrended SSTS an appealing new measurement of small-scale TEC irregularities (SSTI).

ACKNOWLEDGMENTS

The research conducted at the Jet Propulsion Laboratory, California Institute of Technology, is under a contract with the National Aeronautics and Space Administration. This work is partially supported by the Federal Aviation Administration through the Wide Area Augmentation System program. The authors thank the National Geodetic Survey, UNAVCO, and Scripps Institute of Oceanography for making GNSS data available to research communities.

REFERENCES

1. Pi, X., A. J. Mannucci, B. Valant-Spaight, Y. Bar-Sever, L. J. Romans, S. Skone, L. Sparks, and G. M. Hall, Observations of global and regional ionospheric irregularities and scintillation using GNSS tracking networks, *Proceedings. ION GNSS Pacific PNT*, Honolulu, HI, April 2013.
2. A. J. Mannucci, B. D. Wilson, D. N. Yuan, C. H. Ho, U. J. Lindqwister, and T. F. Runge, A global mapping technique for GPS-derived ionospheric total electron content measurements, *Radio Science*, Vol. 33, No. 3, pp.565-582, May-June 1998. https://doi.org/10.1029/97RS02707
3. Iijima, B. A., I. L. Harris, C. M. Ho, U. J. Lindqwister, A. J. Mannucci, X. Pi, M. J. Reyes, L. C. Sparks, and B. D. Wilson (1999), Automated daily process for global ionospheric total electron content maps and satellite ocean altimeter ionospheric calibration based on Global Positioning System data, *Journal of Atmospheric and Solar-Terrestrial Physics*, 61, 1205–1218. https://doi.org/10.1016/S1364-6826(99)00067-X
4. Komjathy, A., L. Sparks, B. D. Wilson, and A. J. Mannucci (2005), Automated daily processing of more than 1000 ground-based GPS receivers for studying intense ionospheric storms, *Radio Science*, 40, RS6006, doi:10.1029/2005RS003279.
5. Sparks, L., Pi, X., Mannucci, A.J., Walter, T., Blanch, J., Hansen, A., Enge, P., Altshuler, E., & Fries, R. (2001). The WAAS Ionospheric Threat Model. *Proceedings of the International Beacon Satellite Symposium 2001*, Boston, MA, June, 2001.6. Zhang, S.-R., Y. Zhang, W. Wang, andO. P. Verkhoglyadova (2017), Geospacesystem responses to the St. Patrick's Daystorms in 2013 and 2015,J. Geophys.Res. Space Physics,122, 6901–6906,doi:10.1002/2017JA024232.
6. Wang, C., Morton, Y., "Ionosphere TEC and TEC Gradients Estimation Using a Regional GNSS Network," *Proceedings of the 26th International Technical Meeting of the Satellite Division of The Institute of Navigation (ION GNSS+ 2013)*, Nashville, TN, September 2013, pp. 1875-1880.